DOI 10.1515/aot-2013-0046 — Adv. Opt. Techn. 2013; 2(5-6): 407–421

Review Article

Wolfgang Fick*, Kai Uwe Gassmann, Luis-Dieter Haas, Markus Haiml, Stefan Hanna, Dominique Hübner, Holger Höhnemann, Hans-Peter Nothaft and Richard Thöt

Infrared detectors for space applications

Abstract: The motivation and intended benefits for the use of infrared (IR) detectors for space applications are highlighted. The actual status of state-of-the-art IR detectors for space applications is presented based on some of AIM's currently ongoing focal plane detector module developments covering the spectral range from the short-wavelength IR (SWIR) to the long-wavelength IR (LWIR) and very long-wavelength IR (VLWIR), where both imaging and spectroscopy applications will be addressed. In particular, the integrated detector cooler assemblies for a mid-wavelength IR (MWIR) push-broom imaging satellite mission, for the German hyperspectral satellite mission EnMAP and the IR detectors for the Sentinel 3 SLSTR will be elaborated. Additionally, dedicated detector modules for LWIR/VLWIR sounding, providing the possibility to have two different PVs driven by one ROIC, will be addressed.

Keywords: AIM; infrared; LWIR; MCT; MWIR; SWIR; VLWIR.

OCIS codes: 040.2480; 040.3060.

***Corresponding author: Wolfgang Fick,** AIM INFRAROT-MODULE GmbH, Theresienstr. 2, D-74072 Heilbronn, Germany, e-mail: wolfgang.fick@aim-ir.com
Kai Uwe Gassmann, Luis-Dieter Haas, Markus Haiml, Stefan Hanna, Dominique Hübner, Holger Höhnemann, Hans-Peter Nothaft and Richard Thöt: AIM INFRAROT-MODULE GmbH, Theresienstr. 2, D-74072 Heilbronn, Germany

1 Introduction

Mankind's exploration 'tool' was initially only the human eye. The range of colors it reveals to us, electromagnetic (e.m.) radiation with wavelengths between 400 nm (color perceived as purple) and 700 nm (red), is referred to as the visible spectral range (VIS), with the human eye capable of distinguishing between 10 million different colors. Other e.m. radiation covers, for example, radio wave bands at longer wavelengths, which we cannot naturally observe, or X-rays at shorter wavelengths, just to mention a few. Thus, the way we used to perceive our surroundings in the past was shaped by only a small portion of the electromagnetic spectrum.

Even though humans were able to feel the warmth of the sun in the sky or the heat originating from a fireplace or a sufficiently hot object, thanks to receptors in our skin, it was not until about 200 years ago that thermal radiation was formally described – the birth of the concept of infrared (IR) radiation with wavelengths larger than those of visible radiation. Today, we distinguish somewhat arbitrarily between the near IR (NIR, 0.7–1 μm wavelength), the shortwave IR (SWIR, 1–3 μm), the midwave IR (MWIR, 3–6 μm), the longwave IR (LWIR, 6–12 μm), the very long wavelength IR (VLWIR, 12–30 μm), and the far IR (FIR, 30–100 μm). This classification is partially derived from technological aspects such as useful atmospheric optical windows (MWIR, LWIR) with large IR transmission, and other nomenclature associated with different wavelength spans exists in the world of fundamental science.

Each of these different IR bands allows us to observe different aspects of the world around us. In order to do this, the spatial proximity to the studied object is not necessarily required (remote sensing). Whereas the FIR permits the analysis of, for example, cold stellar objects in deep space, the NIR to VLWIR bands allow atmospheric absorption bands to be probed and are, therefore, essential for weather and climate monitoring from on board satellites. Tracking the thermal emission of hot objects in the MWIR, like wild fires, is a task that can be performed with IR sensors from space or from airborne platforms. Also geoprospecting characterizing the spectral features of ground formations in the SWIR is feasible using IR detectors.

In order to make use of the IR portion of the electromagnetic spectrum, various kinds of sensors were developed, transforming IR radiation impinging on the sensor and not directly accessible to our eye into electrical signals expressed as voltages or currents. These electrical signals can, in turn, be visually displayed, creating IR screen images of our environment (imaging applications),

involving sophisticated pre- and/or postprocessing of the electrical data. Also, radiometry became possible, which is the quantitative measurement of the IR light intensity reflected and/or emitted by an object as a function of wavelength (color). This is generally performed using either spectrally dispersive apparatuses separating the incident broadband IR light into an often large number of discrete spectral channels for analysis (hyperspectral imagers) or by Fourier transform IR (FTIR) spectroscopy.

In either case, IR sensors sensitive over a particular spectral range in the IR are required. For high-performance applications, HgCdTe (mercury cadmium telluride, MCT) is often used as photosensitive material. Its IR sensitivity range can be tailored to specific wavelength ranges adjusting the material composition, making the IR spectrum between the VIS and the VLWIR accessible. For large detector signal-to-noise ratios, the detectors are usually cooled to temperatures between 40 K and 180 K using mechanical coolers. The photosensitive MCT-sensing layer is structured as p-n junction photodiodes arranged as a pixel array. This array is fused to a CMOS silicon read-out chip, which generates an electrical output voltage proportional to the incident IR photon flux for each picture element. The composite of the photosensitive MCT detection layer and the silicon read-out chip is then referred to as a focal plane array (FPA), which constitutes the key element of any IR instrument.

The sensors can be passive (i.e., not actively illuminating the scene) sensors with photosensitive elements (pixels) lined up in one or a few pixel rows in the focal plane of an optical system (linear array imagers), or they can be two-dimensional sensor arrays. Linear array imagers, in general, require a scanning mirror to sweep the spatially extended object to be examined over the sensor array for detection.

One type of passive scanner is a push broom scanner or along-track scanner used with satellites. It does not have a scanning mirror. Instead, an optical imaging system projects a scan line image from a track on the ground, with the scan line orthogonal to the satellite's flight direction, onto the linear detector array. This is the electro-optical counterpart of leaving straight tracks with a push broom pulled along in a sand box. Each pixel of the sensor array, thus, records, spectrally integrated over the detector's sensitivity range, the signal received from a certain area on the ground (ground pixel). For each spectral band, a separate linear array is required to obtain spectral information. An example of an AIM INFRAROT-MODULE GmbH (AIM) MCT sensor for push broom imaging in the 3 to 5 μm MWIR spectral range from on board a satellite will be presented in section 2.

Large two-dimensional pixel arrays with pixels located on a Cartesian grid are suitable for use with hyperspectral imagers: Here, the pixels in the different sensor array columns, for example, are used to map the signal obtained from different ground pixels and, therefore, store spatial information. Each detector column thus corresponds to a single ground pixel. Dispersive elements (gratings, prism, and grisms) in the instrument optics can spatially separate the spectral content in the signal received from a ground pixel onto the detector pixels of an array row, for example. Therefore, a column of detector pixels stores a spectrum of light obtained from a single ground pixel, with each row within this column addressing a different small spectral bandwidth within this spectrum. An example of an AIM MCT sensor for hyperspectral imaging in the 0.9 to 2.5 μm NIR/SWIR spectral range from on board a satellite will be presented in section 3.

Spatial imaging in a manifold of discrete spectral bands ranging from the SWIR to the LWIR from on board a satellite is achieved using satellite-based AIM sensors as described in section 4, and sensors for use with Fourier transform spectroscopy will be presented in section 5.1.

2 MWIR Push-broom imager

The MCT MWIR detector discussed in the following has been designed for the detection of forest fires and the observation of volcanic activities in a high-resolution push-broom imaging satellite mission.

AIM was contracted to develop and manufacture the high-performance 3 to 5 μm MWIR detector module as part of the satellite payload. The development included the adaptation of existing designs and also completely new developments according to the specific demands and resulted in an integrated detector dewar cooler assembly (IDDCA, see Figure 1), consisting of

- the MCT focal plane detector array (FPA)
- housed in a dewar
- a long-life pulse-tube cooler with an SF400 flexure bearing compressor [1]
- cooler driver electronics (CDE), and
- front-end electronics (FEE)

The cryo pulse-tube cooler will be in nominal operation at all times during the mission providing a highly stabilized temperature for the FPA in its operating point. The flexure bearing compressor is driven and regulated by the CDE, which supplies electrical power, drives the compressor of the cryo pulse-tube cooler, and processes

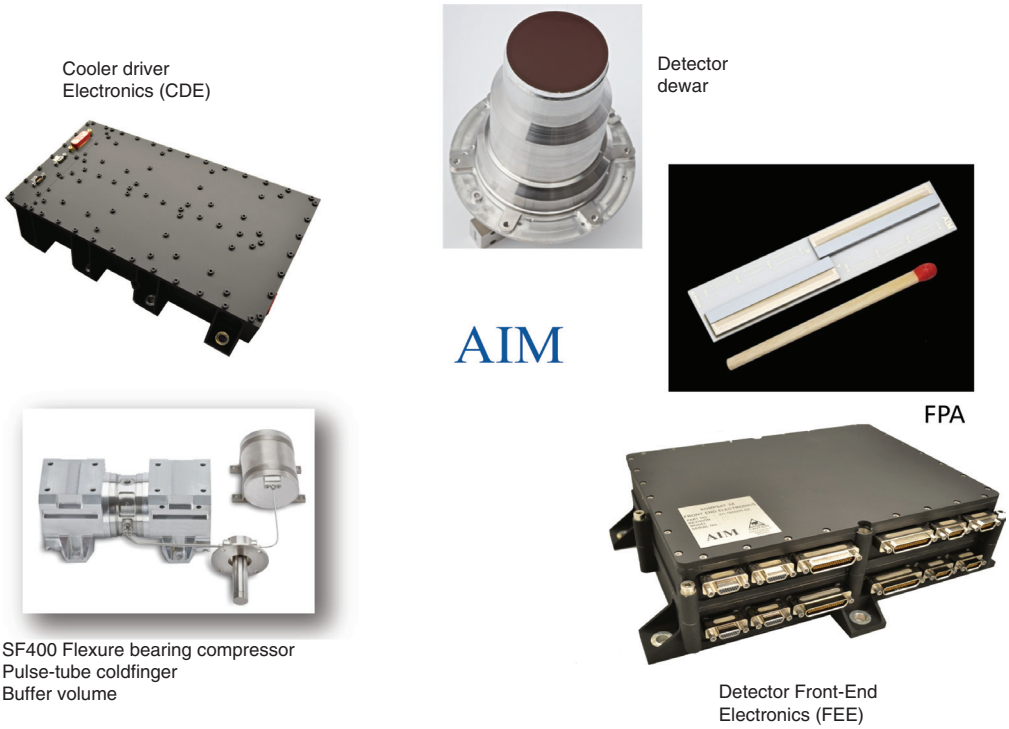

Figure 1 IDDCA components for the MWIR push-broom imaging detector provided by AIM.

temperature-sensor data. With identical functionalities inside the CDE crate, a nominal and a redundant circuit are implemented for risk mitigation.

Incident photons in the MWIR wavelength regime are converted into an electrical signal in the FPA, which is then buffered (or amplified) with pre-amplifiers close to the sensor chip. A time delay and integration (TDI) operation is implemented to gather more light from the same scene by scanning a ground pixel several times and, therefore, to improve the signal-to-noise ratio (SNR). The mean noise-equivalent temperature difference (NETD) for a 293 K blackbody scene is 12 mK at a frame rate of 1300 Hz. The key parameter of the IDDCA is given in Table 1.

The nonlinearity *NL* of the detector is median output signal level S^{median} over all pixels compared to a reference video level S^{fit}, which is derived from a least mean square linear fit to the data, with respect to the integration time T_{int} of the useful signal range ΔS^{useful} between the minimum offset video level (OVL) and the saturation level (ΔS^{useful} ~14 000 $LSB_{14\ bit}$). The maximum nonlinearity is <0.2%.

The FEE supplies all the necessary bias voltages and control clock signals to the detector. Several housekeeping functions are implemented, monitoring voltages, currents, and temperatures. It also converts the detector output signals into a digital data stream and can be used to perform a gain and offset correction. The FEE performs the TDI operation by FPGA-based time-delayed summation of the digital data. Through the multiple sampling of a ground pixel (dependant on the number of TDI pixels) and the summation of the digital data, a higher signal level can be achieved, which is comparable to a longer integration time without additional smearing effects. The linear detector consists of two staggered linear sensors with more than 1200 pixels each. The detector is designed for a line rate with 1000–1500 lines/s and is able to cover a high dynamic range by using high sensitive input capacitive transimpedance amplifier (CTIA) stages for the ambient temperature range (low photon flux) and the low gain direct injection (DI) input stages for the high temperature range (high photon flux) and hot spot detection. Besides the high and low temperature modes, there is an 'image fusion mode' available. Depending on the incident photonic signal level (threshold is programmable), the detector switches the active pixels between highly sensitive pixels and low gain pixels individually for any ground pixel. The advantage of the 'image fusion mode' is to combine the high SNR of the sensitive CTIA pixels with the high dynamic range of the DI pixels.

In 2012, AIM delivered two flight models to be implemented in the satellite, which will operate from a polar low earth orbit. The launch is anticipated for late 2014.

Table 1 The key parameters of the 1200×8 MWIR push-broom imager.

Group	Feature/Description
Spectral range	3–5 μm
Operation temperature	80–90 K
Cryo-cooler type	Pulse-tube/AIM SF400 flexure-bearing compressor
Geometry	>1200×8+1200×8 pixels
	20 μm×20 μm pixel pitch
Pixel input stage	CTIA×7 (low-flux operation)
	DI×1 (fire channel, high-flux operation)
Gain	Switchable between high and low gain for CTIA
Operation modes	Snapshot; integrate while read (IWR)
Pixel deselect	Yes, for any pixel
Frame rate	1000–1500 lines/s
Command and control electronics	2×4 video channels with independent operation
	14-bit cameralink-like video data interface
	Integrated timing generation and bias supply
	Image fusion mode (alternating CTIA, DI) and housekeeping
CDE	$28V_{DC}$±2V with housekeeping and filter

3 Environmental mapping and analysis program (EnMap)

In this section, the 1024×256 pixel shortwave IR HgCdTe (MCT) (SWIR 0.9–2.5 μm) detector will be presented. It is the dedicated SWIR sensor for the German Environmental Mapping and Analysis Program (EnMAP) mission [2], which is a joint effort of German earth observation institutes and the space industry in order to gain quantitative information about the evolution of terrestrial ecosystems. The scientific lead is with the Geoforschungszentrum (GFZ) Potsdam. The mission objectives are the global determination of ecosystem parameters as well as to provide analysis capability after natural disasters and for environmental pollution of land and water and to resolve and detect biophysical, biochemical, and geochemical variables in distinct detail [3]. For this purpose, hyperspectral imaging data covering wavelengths from visible to shortwave IR is acquired. The IR detector array, covering the SWIR region between 0.9 and 2.5 μm will be addressed here. The basic idea of hyperspectral data is shown in Figure 2. The instrument is a push-broom imager, with the second dimension of the detector array used to map the spectral information leading to the desired hyperspectral data set.

The detector with its 1024×256 pixels is especially designed to cope with the needs of a hyperspectral application. The direction of the 1024 pixels with a pixel pitch of 24 μm is used for the lateral resolution of the ground pixels. The spectral information of a ground pixel is dispersed in the direction of the 256 pixels (32 μm pitch). Owing to the nature of spectral data, each of the 256 spectral lines can be set individually into a low or high gain mode in order to cover a high dynamic range of input signals. Depending on the probed sample, each individual line can be turned off on-chip for reduction of the data volume from irrelevant spectral lines. The silicon readout integrated circuit (ROIC) is optimized for measurement of low photon fluxes with frame rates of up to 250 fps. Owing to the electro-optical performance requirements, the operating temperature of the detector hybrid can be set in the range of 120–180 K, with a nominal operating temperature of 150 K. Thus, the detector has to be placed in an evacuated dewar using antireflection-coated sapphire as entrance window. For the cooling system, a long life flexure bearing compressor 'SF100' with a pulse tube [4] is foreseen in order to provide the dedicated detector temperature with a long-term temperature stability of 20 mK.

The resulting system including all electronics is shown as block diagram in Figure 3. The actual hardware without showing the cooler control electronics (CCE) and the detector control electronics (DCE) is shown in the lower left part of the image. The 1024×256 SWIR detector mounted on a structured ceramics placed inside the vacuum dewar is depicted in the lower right, also indicating the orientation of lateral and spectral axis.

For hyperspectral imaging applications, there are several electro-optical key requirements a detector has to fulfill in order to cope with the needs of the mission. These requirements are linearity, quantum efficiency, homogeneity, and readout noise.

The intensity of the spectral bands is crucial information for data evaluation, and thus, the linearity of the detector with respect to photon flux is one of the key

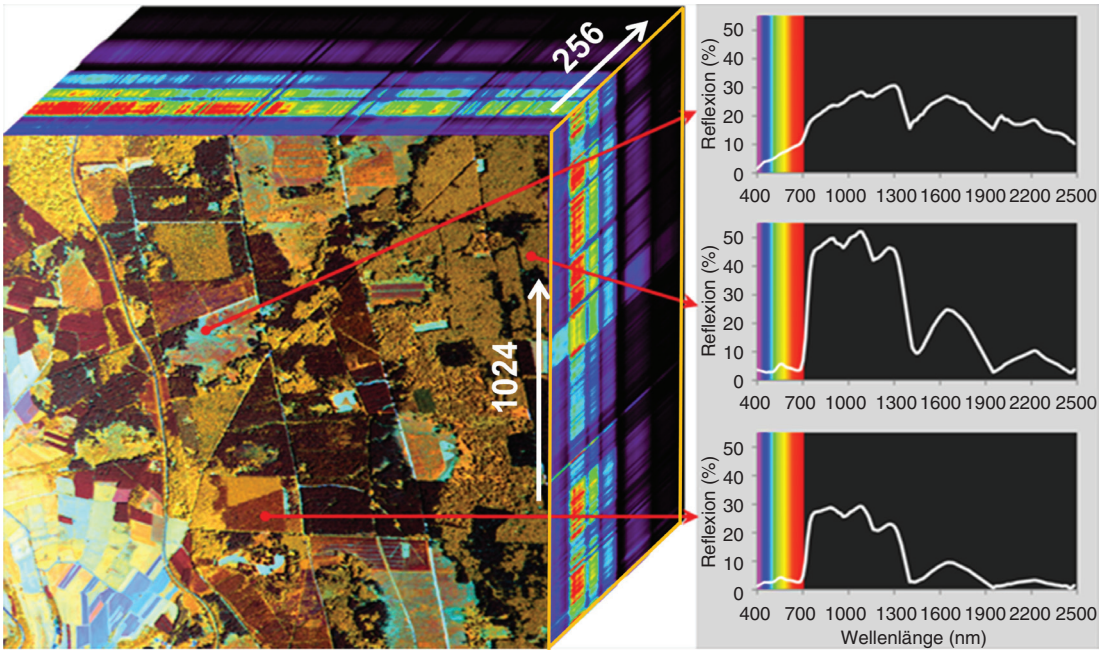

Figure 2 The principle of a hyperspectral data cube is shown. An image consist of frames with the lateral information in the 1024 direction and the spectral information in the 256 direction. For three exemplary points of the image, the according spectra are shown. Source: http://www.uni-trier.de/index.php?id=40541 ('Hyperspectral Cube' einer Waldszene bei Morbach mit 3 Reflexionsspektren).

parameters. The linearity can be measured both as function of photon flux and as function of the integration time, where those results lead to the conclusion that the measurements with respect to integration time can be very well used for calibrating the photon flux data sets. In Figure 4, for an arbitrary pixel, the result of a linearity measurement as function of photon flux is shown. Between 1% and 90% full well, a least mean square linear fit (black9 is applied to the measured data (red). A linear correction is leading to a nonlinearity (referenced to the measured signal) well below 2%, where the origin of the nonlinearity is well understood and localized in the analog signal path of the silicon readout circuit. Thus, the nonlinearity is highly stable over time and pixels leading to the fact that a polynomial function of third degree can be applied as corrective function leading to a nonlinearity below 0.2%.

For hyperspectral imaging, knowledge of the spectral behavior of the detector is mandatory in order to deduce a quantitative analysis of the measured data set. Thus, the spectral responsivity was characterized resulting in the quantum efficiency as function of incident wavelength for each pixel. The normalized spectral responsivity for the detector in the range between 0.7 µm and 2.85 µm wavelength measured at 150 K is shown in Figure 5. The data was taken using a grating spectrometer with calibrated reference detectors. The sharp cut-on of the spectrum originates from the transmission spectrum of CdZnTe substrate, whereas the cut-off wavelength is determined by the composition of the MCT. It can be deduced from the linear increase of the responsivity with wavelength that the quantum efficiency between 0.8 µm and 2.5 µm is constant for the AIM SWIR detector and above 80%. Driven by the application, the homogeneity and the distribution of the cut-off wavelength are also crucial performance parameters. Excellent results for the 2.5-µm cut off with a variation of <0.01 µm for the 1024×256 array are achieved.

This also contributes to the global homogeneity of the detected signal, the photo response non-uniformity (PRNU). This performance parameter is defined as the deviation in percent for each individual pixel from the mean signal of the array under homogeneous illumination conditions. An image of the PRNU (Figure 6) shows that this parameter is well within the boundaries of ±5%.

The above shown key performance parameters together with a read out noise of 150 e^- (high gain) and 290 e^- (low gain) lead to a SWIR detector unit, which perfectly matches the needs of a hyperspectral mission.

The key parameters of the 1024×256 SWIR detector are given in Table 2.

4 Sentinel 3

Besides the shown applications for focal plane arrays as imaging or hyperspectral detectors, there is another concept, which has been applied over several years for

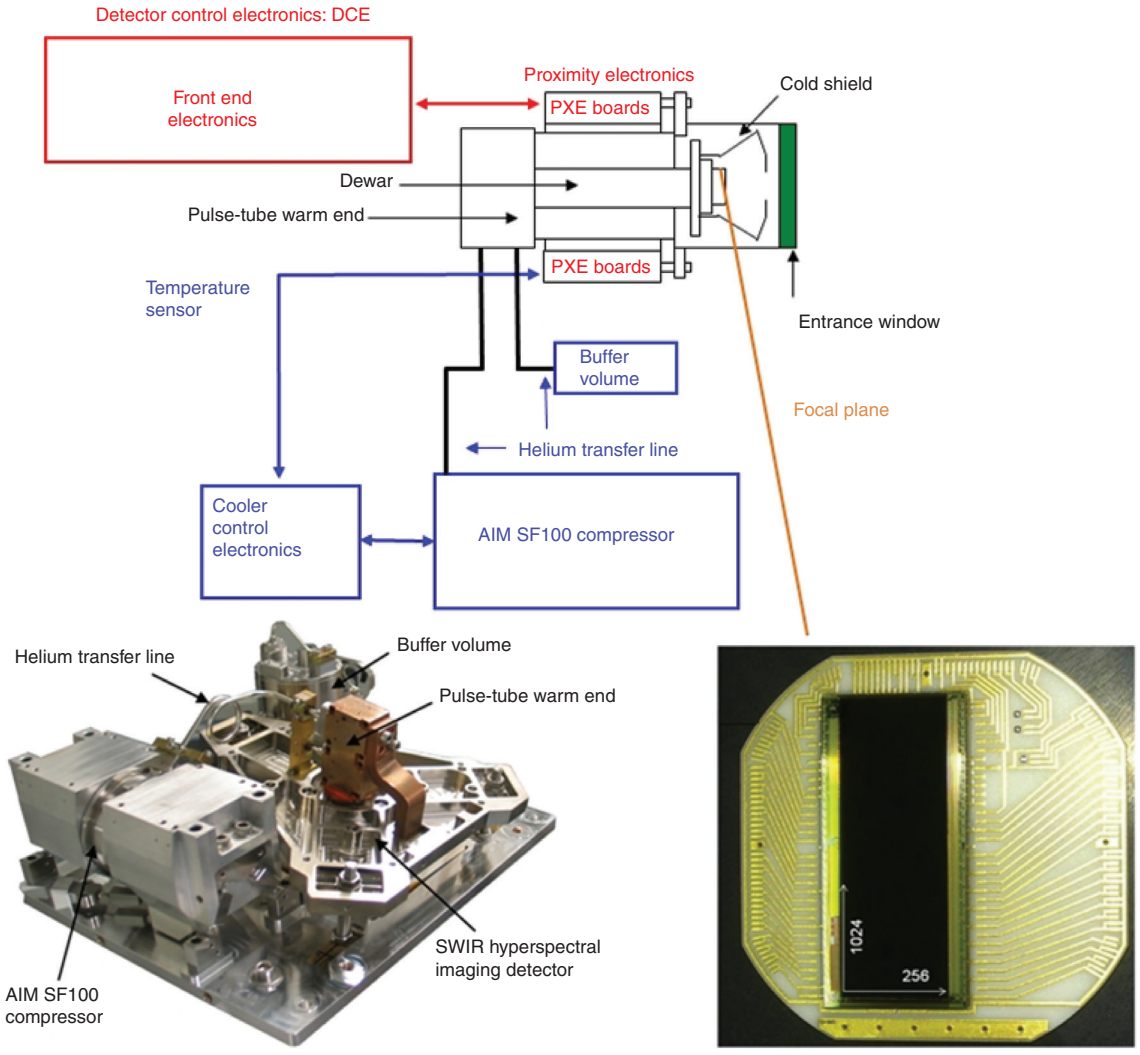

Figure 3 The block diagram of the detector assembly in the upper part depicts all subcomponents including the electronics for the cooling system and the supply and readout electronics for the detector hybrid, shown in the lower right. The image of the hybrid indicates the orientation of the 1024 lateral and 256 spectral pixel of the EnMap MCT SWIR FPA. In the lower left, the detector assembly, consisting of the SWIR hyperspectral imaging detector mounted on a base plate together with the cooling system consisting of a SF 100 compressor with pulse tube, helium transfer lines, and the buffer volume, is shown.

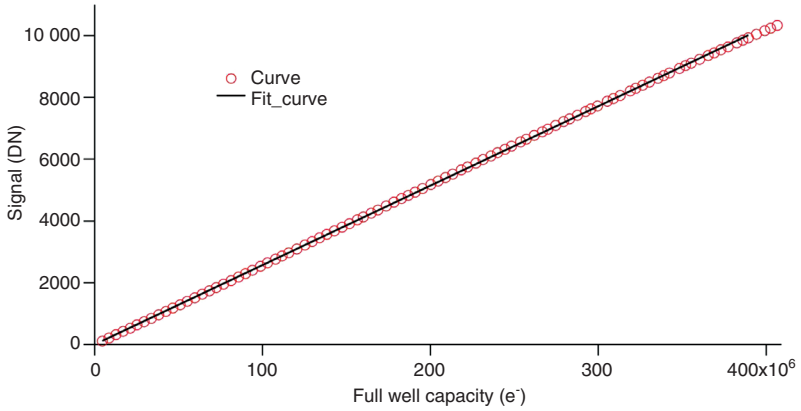

Figure 4 Linearity of the EnMap 1024×256 SWIR detector measured between 1% and 90% of integration capacity filling as a function of photon flux. The measured data is represented by the red data points, whereas the black line indicates the result for the linear fit to the data. The resulting nonlinearity is well below 2%.

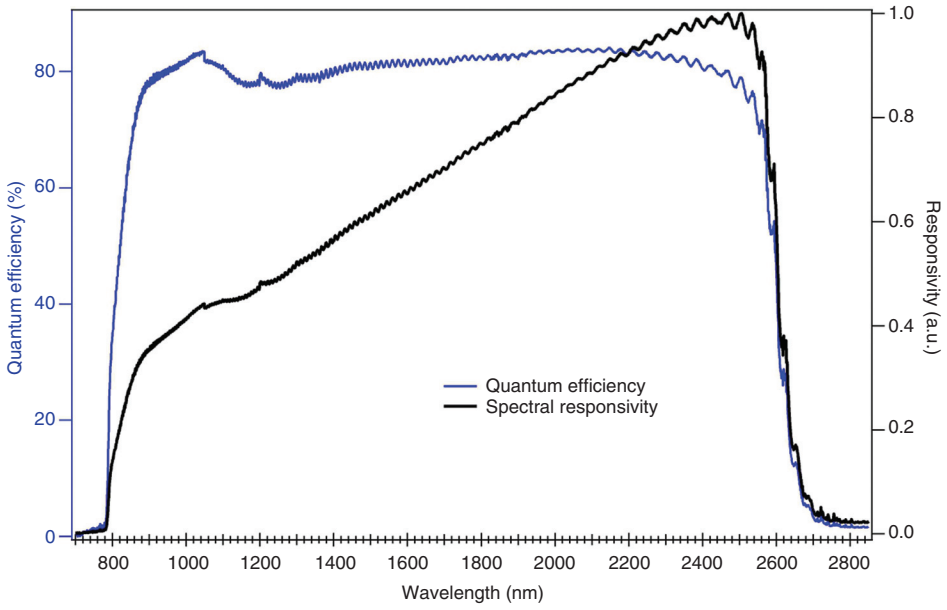

Figure 5 The normalized spectral responsivity is shown in black in a wavelength range between 700 and 2900 nm along with the resulting quantum efficiency of 80% of the EnMap 1024×256 SWIR detector.

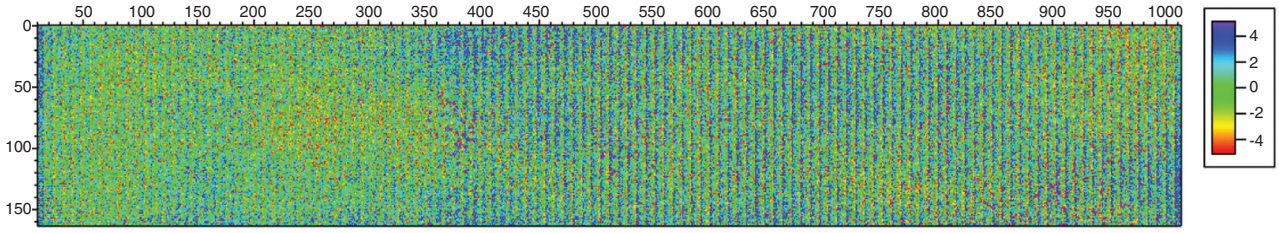

Figure 6 The Photo Response Non-Uniformity (PRNU) is shown in the range of ±5%.

earth remote sensing: the multiband spectrometers. For this concept, the observed radiation spectrum is devided in several small channels, which are treated by different detectors.

This concept was introduced for Earth monitoring with the ATSR instrument launched in 1991 on the Earth Remote Sensing Satellite 1 (ERS-1). Here, four channels with center frequencies at 1.6 µm, 3.7 µm, 11 µm, and 12 µm were selected for several temperature-monitoring tasks to provide a continuous database for climate research.

The concept was continued by the Advanced Along Track Surface Radiometer (AATSR), which operates from on board the ENVISAT satellite, the former flagship of the ESA satellites.

Within the frame of the ESA COPERNICUS program, the Sentinel satellites were defined, each of them covers a special topic in Earth observation. The Sentinel 3 satellite was designed to provide continuous data of the earth's surface temperature to continue the long-term global acquisition of data for climate science. On board this satellite, the Sea and Land Surface Temperature Radiometer (SLSTR) instrument is the direct successor of the AATSR and foreseen to maintain the database for surface surveillance.

Among the spectral channels given by the successor instrument AATSR, two additional shortwave channels were introduced to improve the atmospheric data available to compensate impacts from clouds and atmosphere condition. Dedicated fire channels were introduced to handle high photon fluxes originating from high-temperature events.

The Sentinel 3 SLSTR instrument has three visible channels (S1–S3) and six different IR detector channels S4–S9 covering the spectrum between SWIR and LWIR. With the demonstrated background for each wavelength range, AIM was selected to produce and deliver all the different IR detectors for this instrument. For the SWIR and MWIR channels, the detectors were produced as HgCdTe

Table 2 The key parameters of the 1024×256 SWIR detector.

Group	Feature/Description
Spectral range	0.9–2.5 μm
Operation temperature	120–180 K
Cryo-cooler type	Pulse Tube Coldfinger/SF 100 Flexure Bearing Compressor, Stirling [4]
Detector array geometry	1024×256 pixels
	Spatial direction 1024 pixels, 24 μm pitch
	Spectral direction 256 pixels, 32 μm pitch
	Fill factor >93%
Pixel input stage	CTIA
Gain	Switchable between >0.45 Me^- (high gain) and >1.4 Me^- (low gain) full well capacity
	Gain selection memory: 256 bit register, each spectral line can be deselected individually
Readout noise	High gain: 140 e^-
	Low gain: 290 e^-
Operation modes	Snapshot; integrate while read (IWR), integrate then read (ITR)
Subframe capability	Subframe window (rectangular)
	Row selection memory: 256 bit register,
	Each spectral line can be deselected individually
Integration time	IWR: 0.001 ms–4 ms (full frame) shorter for subframes
	ITR: 0.001 ms–6.5 ms (independent of subframe size)
Pixel clock	7.5 MHz
Video outputs	8 analog
Logic	Digital logic on ROIC generates all clock patterns from external master clock
	Programmable data: operation modes, integration time, row selection, gain selection

photodiodes with Si-based readout electronics to multiplex the pixel to one signal line. The LWIR detectors were developed on the base of HgCdTe photoconductive elements. In Figure 7, the schematic design of the optical bench is given. The light coming from the scanning mirrors (OME) is split several times to feed the different detectors for the various wavelengths. The basic characteristic of the different IR channels is given in Table 3.

The SLSTR instrument is a whisk-broom imager. This means that it is constantly scanning a small stripe of the surface while flying across the Earth. The basic principle is given in Figure 8. The SLSTR has a wide aperture opening, the surface is scanned using a rotating mirror, which is projecting the surface segment to the optical bench. The direction of the view can be switched between Nadir and oblique (rear) mode. The width of the swath is 1400 km or 740 km, respectively. The ground pixel size is dependent on the channel and is 500 m to 1 km. To acquire the data in this approach, the detector itself is only a small array of a few pixels, which will be read out at high frame rates. For the Sentinel 3, the ground pixel size of 500 m or 1 km is projected to a detector pixel size of 100 μm and 200 μm, respectively. The detector design of the shortwave detector units and the longwave detector units is shown in Figure 9.

The detector units are mounted on the optical bench of the instrument, which is cooled down to 80 K operating temperature. The complete detector unit is held at these low temperatures. Therefore, the whole design is dedicated to work stable for a long time at these low temperatures.

Each detector includes a flexible cable as part of the link to the FEE. This flexible cable operates at cryogenic temperature on the detector side and at room temperature on the connector side. It is designed to feed the detectors with lowest parasitic elements and minimize the thermal load of the cooled optical bench. The base material of this flex cable is KAPTON, which is suitable for low-temperature operations. Copper lines are used for the signal nodes. The shielding is gold coated to minimize radiation effects (thermal loads). Each detector was applied with a dedicated layout for the flex cable. A sample design is given in Figure 10.

The key parameters of the six detectors are given in Table 3. For each channel, a common housing and mechanical interface is used. Channel-specific variations are done on the detector units and the optical interface. Figure 11 shows a set of the Sentinel 3 IR detectors. Within the housing, a channel specific-cold shield is aligned to the detectors. The entrance window is optically coated defining the spectral filter for each channel.

With the given instrument concept, the photon flux impinging on each detector is about two decades lower than for typical focal plane applications. To achieve the required performance, a front-side illumination approach for the IR detectors was chosen. In comparison

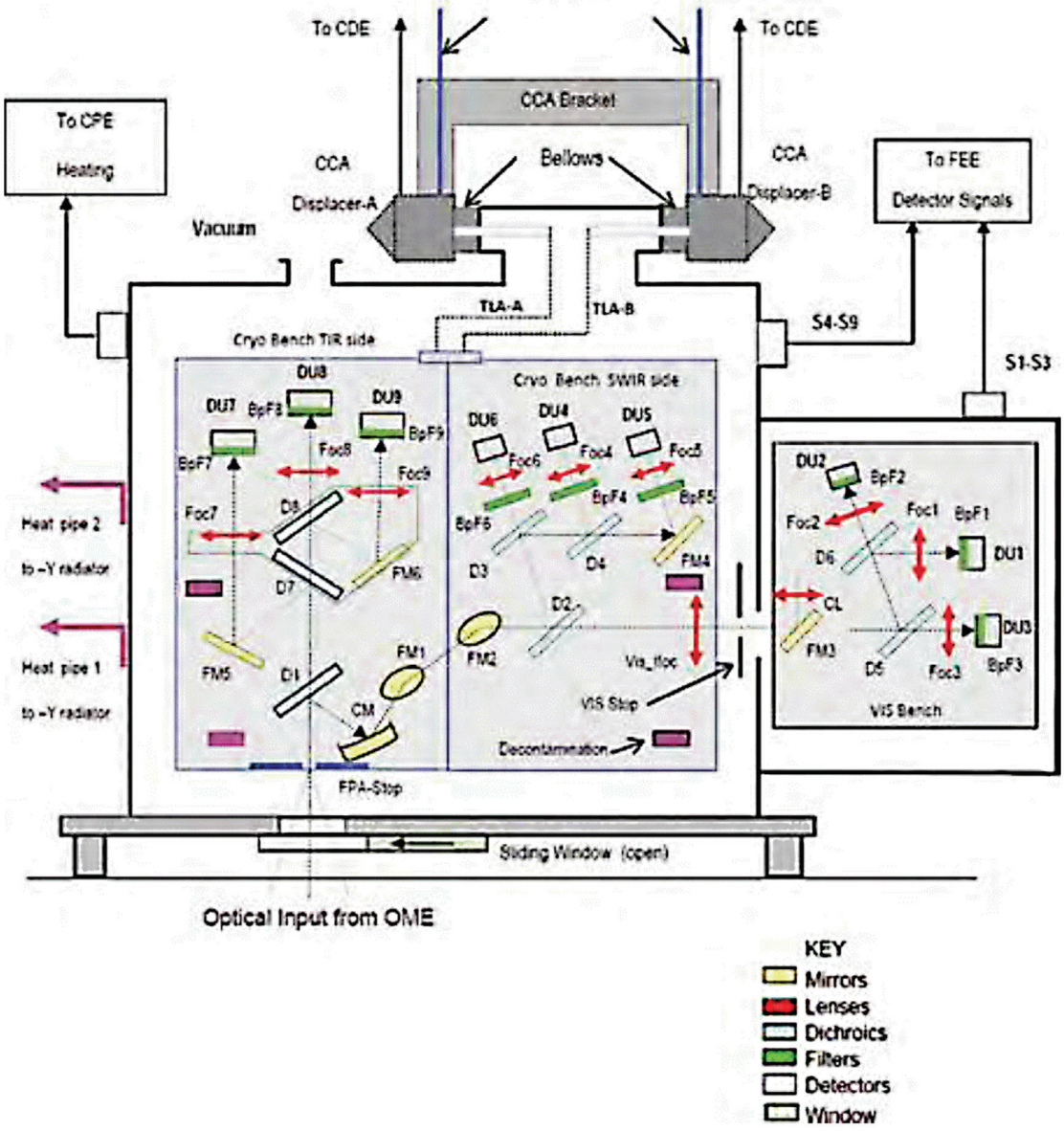

Figure 7 Schematic design of optical bench of the Sentinel 3 SLSTR.

to a standard hybrid approach, all photons are collected directly at the surface of the MCT detector, and the photon loss in the bulk is minimized. Entrance filters having high transmission values around 95% were used. For the PV SWIR and MWIR devices, global QE values of about 80% could be achieved.

For the SLSTR, two dedicated fire channels were installed. One of them is in the MWIR channel S7, where two different detector geometries are combined with different readout stages. While the standard channel is feeding a CTIA input stage, the fire channel is using a BDI integration stage. By this configuration, the operational photon fluxes can vary by about six decades. All PV channels have an antiblooming circuitry to prevent saturation effects due to hot spots. The image lag between fully saturated and dark pixels is below 1%.

Although the detector arrays are very small, the large pixel size together with the high frame rate is a challenge for the readout electronics. Good linearity with non-linear error values below 1% could be achieved for output signal levels up to 95% of the full well by variation of the integration time. The non-linearity error is defined as the deviation to the linear fit relative to the useful signal swing. A sample plot for one 1.6-µm channel is given in Figure 12.

Owing to the mechanical design of the housing, the background radiation for the longwave PC detectors could be reduced significantly. Therefore, even for this type of

Table 3 The key parameters of the different Sentinel 3 IR channels.

3 SWIR channels:	S4	λ_{c4}=1.375 µm	PV, 4×2 array, 100 µm×100 µm pixel size
	S5	λ_{c5}=1.61 µm	PV, 4×2 array, 100 µm×100 µm pixel size
	S6	λ_{c6}=2.25 µm	PV, 4×2 array, 100 µm×100 µm pixel size
1 MWIR channel:	S7	$\lambda_{c7\text{-}1}$=3.74 µm	PV, 2×1 array, 200 µm×200 µm pixel size
	Fire channel	$\lambda_{c7\text{-}2}$=3.74 µm	PV, 4×1 array, 100 µm×25 µm pixel size
1 LWIR channel:	S8	λ_{8}=10.85 µm	PC, 2×1 array, 200 µm×200 µm pixel size
1 VLWIR channel:	S9	λ_{9}=12.0 µm	PC, 2×1 array, 200 µm×200 µm pixel size
Operating temperature		80 K ... 90 K	
Pixel input stage	S4–S7	CTIA	
	S7 Fire	BDI	
Operation mode	S4–S7	Snapshot; integrate while read (IWR)	
	S8, S9	Bridge configuration	

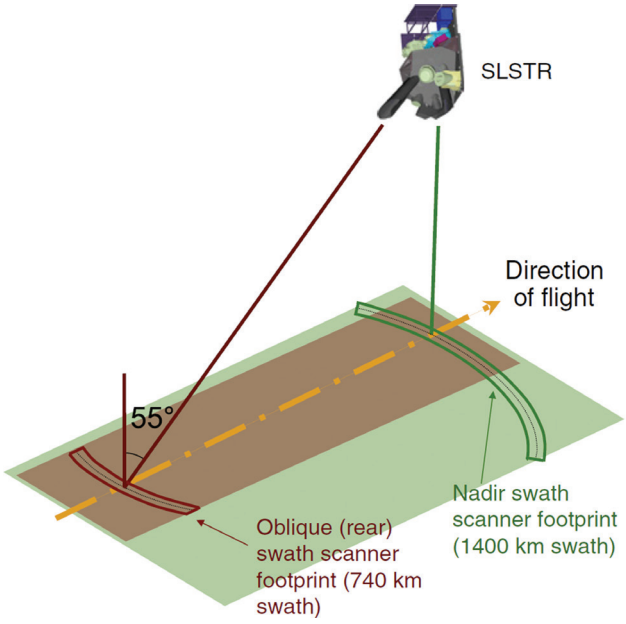

Figure 8 Basic concept of the SLSTR instrument.

detector, a very good linearity could be achieved. The maximum of nonlinearity is about 2.5% for the regular photon flux range. But even for the use as second fire channel, the nonlinearity does not exceed 3% even at very high photon power as shown in Figure 13.

For the PC detectors, a responsivity >150 kV/W could be achieved even at elevated operating temperatures of 90 K.

Four sets of IR detectors have been shipped in 2012 for the first two Sentinel 3 satellites for the integration into the instrument. The launch of the first satellite is expected in 2014 by ROCKOT in Pleseetsk, Russia.

5 LWIR/VLWIR MCT FPAs

5.1 GLORIA

Combining a fast two-dimensional IR detector array with a Michelson Fourier transform spectrometer (FTS) allows registering spectral and spatial information simultaneously. Deployed to space as a limb imaging FTS, three-dimensional distributions of temperature of a large number of trace species such as ozone, water vapor, HNO_3, and climate-sensitive chlorofluorocarbons as well as cloud information can be inferred [5, 6]. The main scientific focus is on the dynamics and chemistry of the upper troposphere and lower stratosphere (UTLS) region. In addition, global observations of gravity-wave momentum fluxes are envisaged [7]. The Gimballed Limb Observer for Radiance Imaging of the Atmosphere (GLORIA) [8, 9] is a joint development of an airborne limb imaging FTS by the German Helmholtz centers JÜLICH and Karlsruhe Institute of Technology (KIT) and was employed on the Russian high-altitude (up to 20 km) aircraft Geophysika and on the German High Altitude Long Range (HALO) research airplane. During the recent TACTS/ESMVAL campaign, GLORIA took more than 100 h of atmospheric measurements observing events of breaking Rossby waves, dehydration in the Antarctic polar vortex, and biomass

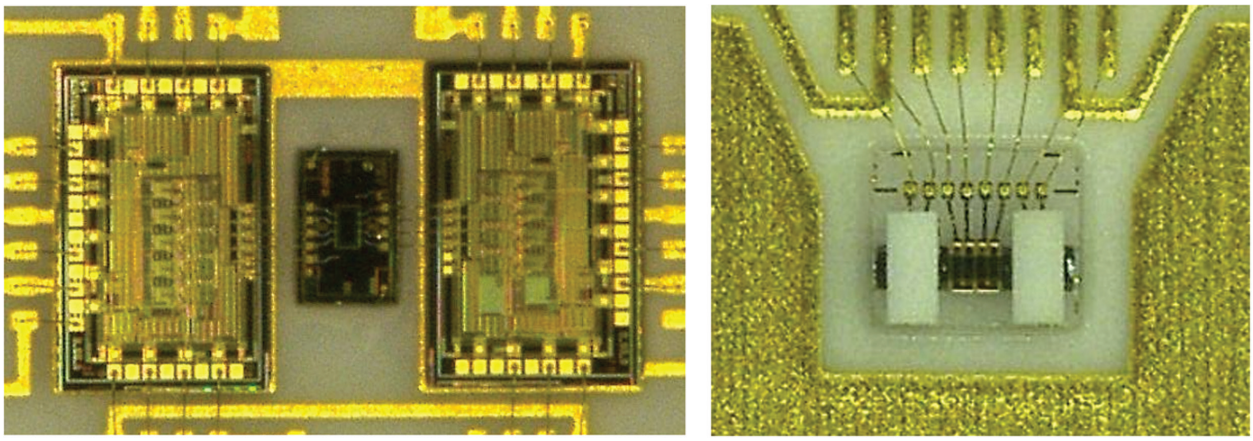

Figure 9 SLSTR detectors for SWIR channels (left) and LWIR channels (right).

Figure 10 SLSTR detector with flex cable.

burning. The GLORIA project has a clear roadmap, starting from laboratory breadboard activities in 2005, performing scientific experiments on Geophysika and HALO with the near future objective to implement a high-altitude balloon experiment, and finally targeting at a space-based limb imaging FTS for climate research.

AIM has developed, manufactured, characterized, and delivered in 2005 a prototype IDCA (Gloria I) for

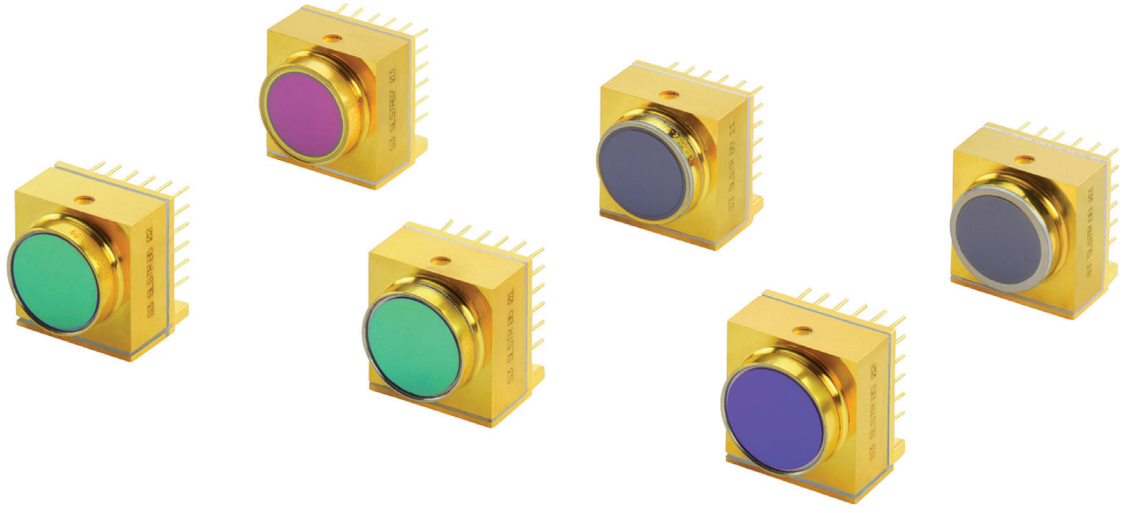

Figure 11 The sentinel 3 IR detector units.

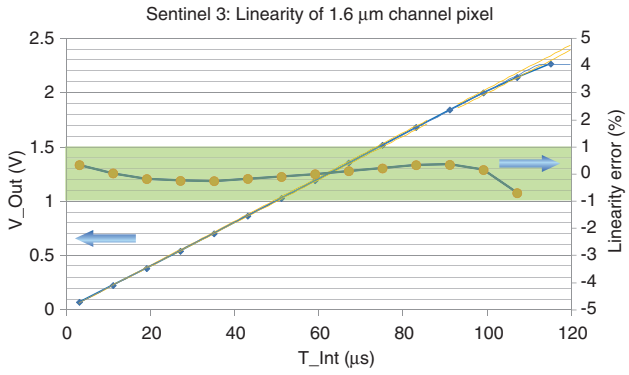

Figure 12 Sample plot of the linearity of a 1.6-µm channel pixel.

laboratory use. The VLWIR MCT FPA key figures are ~13.3 µm cut-off wavelength with 40 µm pixel pitch, 256×256 pixel format, 10×10 mm² active area, 8 analog video channels at up to 10 MHz pixel clock, and nearly 1 Gbit/s data rate at 880 frames/s. The utilized 128×128 subframe is operated at 2.6 kHz, reaching 12 kHz for a 32×32 subframe.

Subsequently, AIM has developed two improved flight units (Gloria-II/1, Gloria-II/2) for the high-altitude airplane experiments. An unprecedented spatial resolution of 30 km (horizontally) and 200 m (vertically) has been achieved with the GLORIA instrument. Gloria-I and Gloria-II have been manufactured utilizing a 0.7-µm ROIC with DI from the 1990s.

Currently, AIM is developing a new detector family (Gloria III) for the high-altitude balloon experiment in close cooperation with FZJ and KIT. The key parameters of the GLORIA III detector are shown in Table 4. The focus of the development is on an update to the ROIC (improved performance and functionality, 180 nm CMOS technology) and on the implementation of two independent PV-arrays on a single ROIC. The 256×256 pixel format and 40-µm pitch is replicated to allow replacement upgrades of the Gloria-II IDCAs in the HALO instrument. The ROIC is

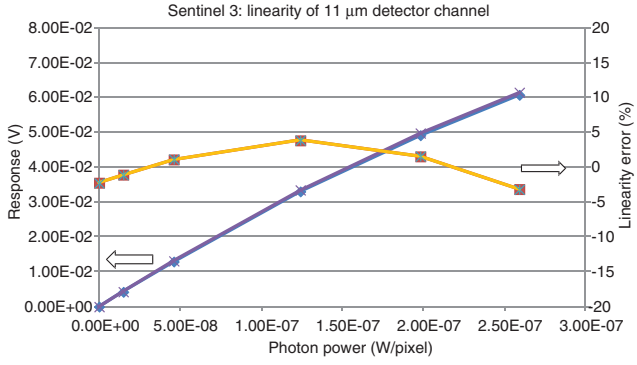

Figure 13 Sample plot of the linearity of an 11-µm channel pixel.

dedicated to operate either with a single 256×256 MCT pv array or with two independent 256×128 MTC pv sub-arrays, allowing different cut-off wavelengths on a single detector, as listed in Table 4 and shown in Figure 14. The implementation of two sub-arrays in one IDCA significantly increases the sensitivity for smaller wavelengths (6–9 µm), while keeping size, weight, power, and costs much lower compared to two individual IDCAs. Both detector halves (9.0 µm/14.7 µm cut-off) can be operated independently with individual integration times, programmable gain (integration capacity), and MCT bias voltages. The gap between active pixels from one sub-array to the other is <500 µm. A buffered direct injection (BDI) is used to collect the photocurrent in each pixel with high linearity, low noise, and sufficient bandwidth. An optimized read-out scheme is implemented to reach 4.8 kHz frame rate for the 128×128 subframe using 16 video outputs. Advanced VLWIR HgCdTe (MCT) material is used, based on extrinsically doped liquid-phase epitaxy (LPE) grown absorber layers for low-dark-current applications [10].

5.2 MTG Predevelopment

Under contract ESTEC 20833/07/NL/FF for the European Space Agency (ESA), AIM has developed, manufactured, and characterized VLWIR MCT FPAs within the Meteosat Third Generation (MTG) phase A predevelopment activities [11–13]. Both the flexible combined IR imager (FCI) and the IR sounder (IRS) instruments were addressed. The IRS test vehicle has been designed as a high-speed two-dimensional detector array for use in spatially and spectrally resolved Fourier transform (FT) spectroscopy in the LWIR/VLWIR spectral ranges.

AIM manufactured a 40 µm×40 µm pixel pitch VLWIR MCT photodiode array in n-on-p technology with a ~14.4-µm cut-off wavelength at 55 K, constituting the photosensitive detection layer. The 112×112 pixels are clustered in groups of 2×2 subpixels forming superpixels, which are each connected to one read-out circuit input stage. The array is thus composed of 56×56 superpixels with an 80 µm×80 µm superpixel pitch (see Figure 15).

The array incorporates a technique for linearity improvement at high photon fluxes in the LWIR/VLWIR, extrinsic p-doping for low dark current, a subpixel select/deselect option and pixel guards for improved spatial resolution. The customized read-out integrated circuit (ROIC) has a full-well capacity (FWC) of 143 mega electrons per superpixel with a buffered direct injection (BDI) input stage and is supporting integrate-while-read (IWR) operation. It provides two independently operating halves with

Table 4 GLORIA III key parameters.

Parameter	Description
Spectral range	Area A: 9.0 µm cut-off/Area B: 14.7 µm cut-off
Operation temperature	50–60 K
Cryo-cooler type	AIM SL400
Detector array geometry	256×256 pixel format; 40 µm pixel pitch
Pixel input stage	BDI input stage
Operation mode	Snapshot; integrate while read (IWR) and integrate then read (ITR)
Gain switch	8 steps, from 2 Me^- to >30 Me^-
Full frame rate	1.8 kHz at 13.3 MHz pixel clock
ROIC technology	180 nm
Special features	Two independently controllable sub-arrays (halves) for control of PVs with different cut-offs (gain, integration time, detector bias)

two analog video outputs each. In full frame, a frame rate of typically 4k frames/s is achieved, making it very suitable for use with rapid scan FT IR spectrometers. Additionally, an in-pixel gain switch is available.

For optimization of detection efficiency, a broadband multilayer LWIR/VLWIR antireflective (AR) coating has been developed with a reflectivity of <7% between 8.0 µm and 14.3 µm. The substrate has been completely removed from the pv chip in order to avoid Fabry-Pérot interferences.

During the electro-optical characterization, the following results were achieved at an operational temperature of 55 K with a ~14.4-µm cut-off wavelength [12]:

- a photo response of 12.1 mV/K
- a noise equivalent temperature difference of 24.8 mK at half-well filling (286 K reference scene)
- The photo response nonuniformity amounted to ~3% (1σ) over the array.
- The nonlinearity error was <0.5%.

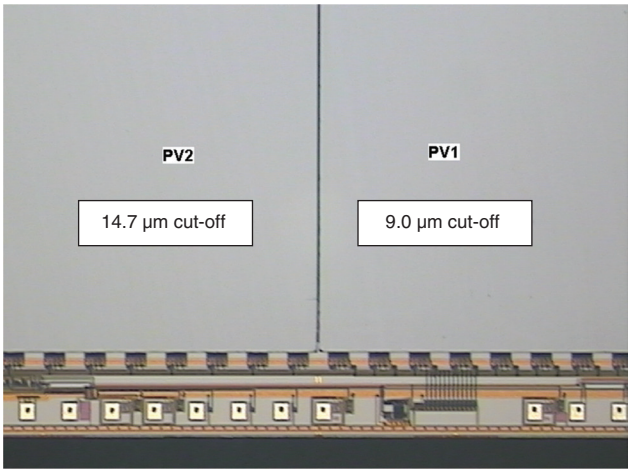

Figure 14 GLORIA III hybrid with two different PV materials hybridized onto a single ROIC.

Dark current densities below 1 pA/µm² and dark signal non-uniformities below 30% are attained in this spectral range.

Especially for radiometric applications and, in particular, for use of the FPA with an FTIR spectrometer, the linearity of the output signal with input photon flux is essential. For linearity testing, the FPA under investigation is at a 55 K operating temperature, and the detector is exposed to a 298 K large area blackbody scene. In order to sweep through the IC filling level and thereby to simulate various illumination conditions, the integration time is varied such that IC filling levels between saturation and starvation are attained, and the output signals of all superpixels are measured with all subpixels activated.

The obtained results are displayed in Figure 16. In Figure 16 (left), the median output signal level S^{median}

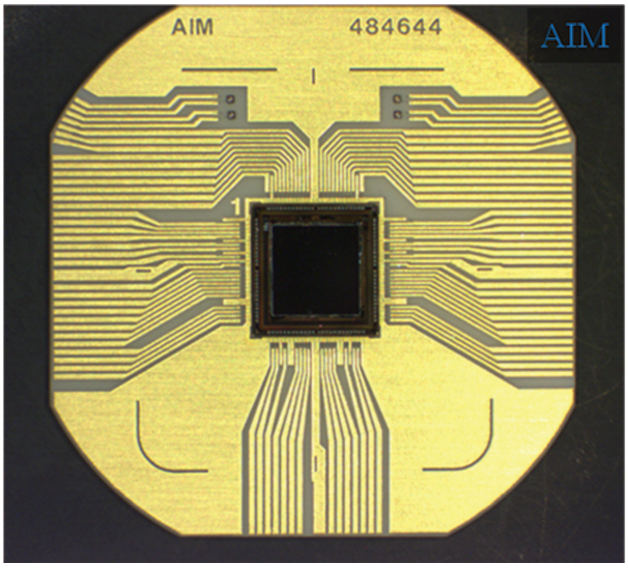

Figure 15 Illustration of test vehicle VLWIR MCT focal plane array for the MTG phase A predevelopment IRS instrument.

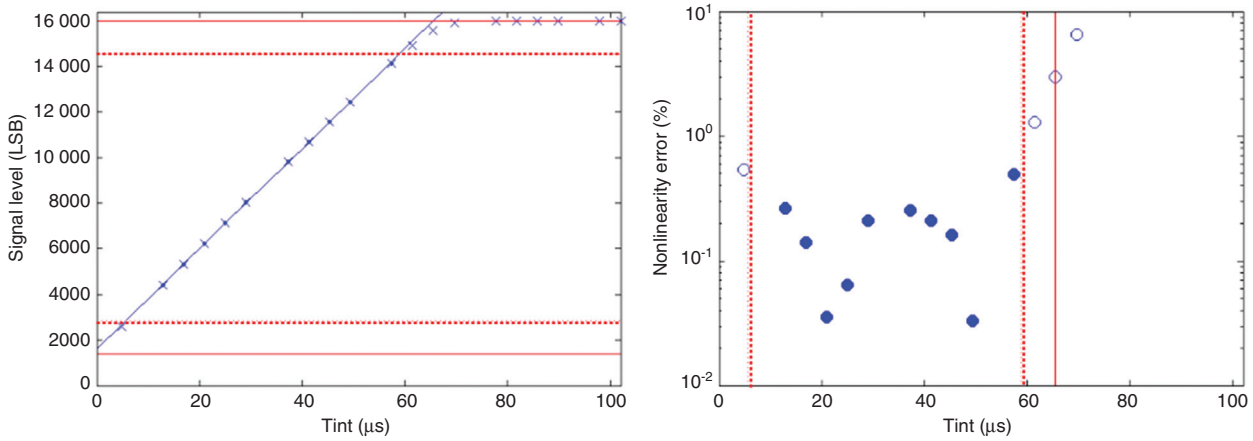

Figure 16 Left: Median output signal level over all superpixels as a function of integration time. Right: Nonlinearity error obtained from the left graph. The nonlinearity error is <0.5% in the range of interest.

over all subpixels of the array is graphed as a function of integration time T_{int}. The horizontal solid red lines define the useful signal range ΔS^{useful} between the minimum offset video level (OVL) with all subpixels deactivated and the saturation level. With a 14-bit analog-to-digital (AD) converter in the external detector electronics used, the conversion factor has been determined as 131.7 µV/LSB. Thus, the useful signal range of ~14 600 LSB corresponds to a useful voltage swing of ~1.92 V. The signal range of interest between 10% and 90% of this useful range is indicated by dotted horizontal red lines. The data points (×) in the range of interest are approximated using a least-mean square linear fit

Equation 1:

$$S^{fit}[LSB]=219.1\times T_{\text{int}}[\mu s]+1628$$

which is represented by the blue solid line. The nonlinearity error *NL* we define as
Equation 2:

$$NL=\left|\frac{S^{median}-S^{fit}}{\Delta S^{useful}}\right|$$

The resulting nonlinearity is graphed in Figure 16 (right). The integration time interval corresponding to the signal range of interest is indicated by the vertical dotted red lines. As expected, the nonlinearity is generally increasing toward saturation and toward starvation. The maximum nonlinearity in the range of interest is 0.49%.

The radiation hardness of the implemented FPA designs has been proven in dedicated γ and proton irradiation campaigns (both on FPA level and under operating conditions) as well as in a heavy ion irradiation campaign (on ROIC level, operating at room temperature) with respect to MTG mission parameters [13].

With all four subpixels per superpixel activated, the pixel guard active and the array at nominal operating temperature, the value of the modulation transfer function (MTF) at Nyquist frequency amounts to 0.70 in both the horizontal and vertical directions as derived from the measured point spread function (PSF) of the detector array presented in Figure 17. Under these conditions, the global detection efficiency is 52%. For comparison, the MTF at Nyquist frequency amounts to 0.51 with guard off).

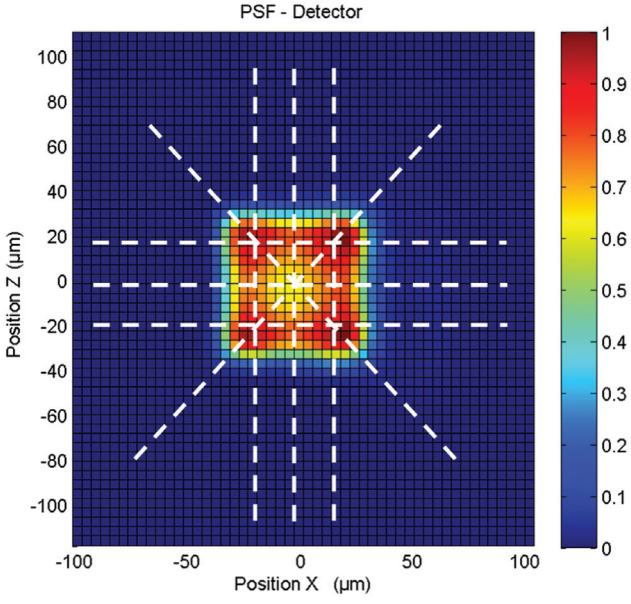

Figure 17 The PSF of the VLWIR MCT focal plane array test vehicle for the MTG phase is shown. The resulting MTF is 0.70 at Nyquist frequency.

6 Conclusion

AIM develops, manufactures, and qualifies integrated detector cooler assemblies and detector electronics for use with space programs in the IR spectral range from 850 nm to 15 µm wavelengths. The detector material is mainly MCT. The silicon readout integrated circuits (ROIC) can be designed upon the requirements of the project providing high performance and features like two different MTC cut-off materials being hybridized onto a single ROIC. An extension to the UV/VIS spectral range is anticipated in the near future. The detector applications cover imaging as well as Fourier transform sounding applications with high spectral and spatial resolution. The first satellite-based detector flight models were delivered in 2012.

Acknowledgments: EnMap is built under contract of the German Space Administration DLR with funds of the German Federal Ministry of Economic Affairs and Technology (50 EP 0801). The work on the MTG phase A predevelopment activities has been supported by the European Space Agency (ESA) under contract ESTEC 20833/07/NL/FF. The support is gratefully acknowledged.

Received August 14, 2013; accepted September 27, 2013; previously published online October 26, 2013

References

[1] S. Zehner, M. Mai, A. Withopf and I. Rühlich, Proc. ICC 17 (Los Angeles), p. 85–92, (2012).
[2] S. Hofer, H. J. Kaufmann, T. Stuffler, B. Penné, G. Schreier, et al., Proc. SPIE. 6366, (2006).
[3] T. Stuffler, C. Kaufmann, S. Hofer, K. P. Förster, G. Schreier, et al., Acta Astronaut. 61, 115–120 (2007).
[4] H. Korf, I. Rühlich, M. Mai and G. Thummes, Proc. SPIE 5783, 164–168 (2005).
[5] M. Riese, F. Friedl-Vallon, R. Spang, P. Preusse, C. Schiller, et al., JASR 36, 989–995 (2005).
[6] F. Friedl-Vallon, M. Riese, G. Maucher, A. Lengel, F. Hase, et al., JASR 37, 2287–2291 (2006).
[7] P. Preusse, S. Schroeder, L. Hoffmann, M. Ern, F. Friedl-Vallon, et al., Atmos. Meas. Tech. 2, 299–311 (2009).
[8] J. Ungermann, M. Kaufmann, L. Hoffmann, P. Preusse, H. Oelhaf, et al., Atmos. Meas. Tech. 3, 1647–1665 (2010).
[9] F. Friedl-Vallon and GLORIA-Team, AIP Conference Proceedings 1531, 308–311 (2013).
[10] R. Wollrab, A. Bauer, H. Bitterlich, M. Bruder, S. Hanna, et al., J. Electron. Mater. 40, 1618–1623 (2011).
[11] S. Hanna, A. Bauer, H. Bitterlich, M. Bruder, M., M. Haiml, et al., Proc. SPIE 7474, 747415 (2009).
[12] S. Hanna, A. Bauer, H. Bitterlich, M. Bruder, L.-D. Haas, et al., Proc. SPIE 7826, 78261H (2010).
[13] A. Weber, W. Belzner, L.-D. Haas, S. Hanna, K. Hofmann, et al. in 'Conference on Radiation Effects on Components and Systems' (RADECS), Sevilla (2011).